Article:
Wang, J., Atallah, K., Chin, R. et al. (2010) Rotor Eddy-Current loss in permanent-magnet brushless AC machines. IEEE Transactions on Magnetics, 46 (7). pp. 2701-2707. ISSN: 0018-9464

https://doi.org/10.1109/TMAG.2010.2042963

Rotor Eddy-Current Loss in Permanent-Magnet Brushless AC Machines

Jiabin Wang[1], K. Atallah[1], R. Chin[2], W. M. Arshad[2], and H. Lendenmann[2]

[1]Department of Electronic and Electrical Engineering, The University of Sheffield, Sheffield S1 3JD, U.K.
[2]ABB Corporate Research, Västerås SE-721 78, Sweden

This paper analyzes rotor eddy-current loss in permanent-magnet brushless ac machines. It is shown that analytical or finite-element techniques published in literature for predicting rotor eddy-current loss using space harmonic based approaches may not yield correct results in each magnet segment when one magnet-pole is circumferentially segmented into more than two pieces. It is also shown that the eddy-current loss in each equally segmented piece may differ by a large margin, which implies that the temperature distribution in the magnets will be uneven and the risk of demagnetization has to be carefully assessed. The theoretical derivation is validated by time-stepped transient finite-element analysis.

***Index Terms*—Eddy-current loss, permanent-magnet brushless machines.**

I. Introduction

PERMANENT-MAGNET (PM) brushless machines have been increasingly used in a variety of applications ranging from high speed manufacturing [1], electric and hybrid vehicle traction [2], [3] to wind power generation [4], [5]. To improve torque density and reduce torque ripple, a new class of PM machines are emerging in which stator coils are wound on consecutive or alternate teeth with a fraction number of tooth per pole [3], [6]. While this winding configuration known as modular is conducive to high efficiency and high torque density, it results in the fundamental magnetomotive force (MMF) having fewer poles than the PM rotor, the torque being developed by the interaction of a higher order stator space harmonic MMF with the field of the permanent magnets. The lower and higher order space harmonics rotating at different speeds to that of the rotor magnets can induce significant eddy currents in the magnets and incur loss [6].

Analytical methods for predicting rotor eddy-current loss in PM brushless machines have been developed in [6]–[10]. They are based on the assumption that the magnets are surface-mounted and the eddy currents are resistance limited, i.e., the relatively high resistivity and low permeability of permanent magnets will limit the amplitude of induced eddy currents and the reaction field produced by the eddy currents is negligible, or the skin depth of the eddy-current distribution is much greater than both the radial thickness and pole arc of the magnets. By formulating the eddy-current problem in the polar coordinate system, the developed methods are applicable to both internal and external rotor machines [6]–[8], [10] and can take into account the effect of circumferential segmentation of magnets and time harmonics in stator currents on the eddy-current losses. The methods have been further extended to linear PM machines [9].

However, for high frequency harmonics or when a metallic retaining sleeve with high electric conductivity is used, the skin depth becomes small and the resistance limited assumption may not be valid. Analytical solutions for rotor eddy-current distribution can also be established by solving the diffusion equation in the polar or Cartesian coordinate systems [11]–[16]. The results are much more complex and as such, the effect of circumferential segmentation of magnets on eddy-current loss has not been considered, or they are only applicable to the rotor topologies in which magnets in each pole are not segmented.

Rotor eddy-current loss can also be predicted by time-stepped transient finite-element (FE) analysis [17]–[19]. To save computation time, harmonic based approaches may also be employed [20], [21] in which eddy-current loss against each rotating space harmonics is calculated as a steady-state ac problem. The total loss is the sum of the losses associated with each harmonic.

In all the analytical or harmonic based FE predictions, the rotor eddy-current distribution is solved for each rotating space harmonic and the resulting eddy-current loss is calculated by summing the loss associated with each harmonic. Consequently, the eddy-current loss in each equally segmented piece will be the same, which has led to believe that the eddy-current loss in each piece is equal. In general, however, this treatment yields correct results only if the frequency of the eddy-current associated with each space harmonic is different from others.

This condition is, however, not true in most PM machines, since forward and backward rotating space harmonics of different orders may yield the same frequency seen by the rotor. To rectify this problem, the rotor eddy-current distribution is formulated in this paper as a sum of space and time harmonics for each frequency and the eddy-current loss is calculated by summing the losses of all frequency components. It is shown that when the magnets in each pole are segmented into more than two pieces, the eddy loss in each equally segmented piece may differ by a large margin, which implies that the temperature distribution in the magnets will be uneven and the risk of demagnetization has to be carefully assessed [22]. The theoretical

Manuscript received October 20, 2009; revised December 21, 2009 and January 19, 2010; accepted January 19, 2010. First published March 08, 2010; current version published June 23, 2010. Corresponding author: J. Wang (e-mail: j.b.wang@sheffield.ac.uk).

Color versions of one or more of the figures in this paper are available online at http://ieeexplore.ieee.org.

Digital Object Identifier 10.1109/TMAG.2010.2042963

derivation is validated by time-stepped transient finite-element analysis.

II. Eddy-Current Loss in Rotor Magnets

To simplify the derivation, the following assumptions are made.

1) Stator and rotor cores are infinitely permeable, and the stator core is slotless.

2) The current distribution in the slotted stator is represented by an equivalent current sheet with a surface current density given by

$$J_s(\theta,t)=\frac{q}{2}\left\{\sum_{n=qk-1;k=1,2,3...} J_n\cos(np_s\theta-p_r\Omega t) - \sum_{n=qk+1;k=0,1,2...} J_n\cos(np_s\theta+p_r\Omega t)\right\} \quad (1)$$

where q is the number of phases, p_s and p_r are the number of pole-pairs of the stator winding and rotor permanent magnets, respectively, θ is the angular displacement on the stator bore, and Ω is the mechanical angular speed of the rotor. J_n is the amplitude of the nth space harmonic given by

$$J_n=\frac{2N_sI_m}{\pi R_s}K_{wn} \quad (2)$$

where R_s is the radius of stator inner bore, N_s and I_m are the number of series turns per phase, and the peak current, respectively, and K_{wn} is the winding factor associated with the nth harmonic. For machines with concentric windings, it is given by

$$K_{wn}=\sin\left(\frac{np_s\pi}{N_{ss}}\right)\frac{\sin(np_s\beta_0)}{(np_s\beta_0)} \quad (3)$$

where N_{ss} is the number of slots and β_0 is the width of the slot opening in radians. It should be noted that the variable reluctance effect due to slot openings is neglected under assumptions 1) and 2). Equation (1) can be further expressed with respect to the rotor reference system as

$$J_s(\theta_r,t)=\frac{q}{2}\left\{\sum_{n=qk-1;k=1,2,3...} J_n\cos[(np_s\theta_r+(np_s-p_r)\Omega t] - \sum_{n=qk+1;k=0,1,2...} J_n\cos[(np_s\theta_r+(np_s+p_r)\Omega t]\right\} \quad (4)$$

where θ_r is the angular position at the stator bore referred to the rotor reference system. For surface-mounted PM machines, the 2-D vector magnetic potential distribution, A_z, in the airgap and magnet regions can be analytically established [10] and is given by

$$A_z(r,\theta_r,t) = \frac{\mu_0 q}{2}\left\{\sum_{\substack{n=qk-1\\k=1,2,3...}}\frac{J_n}{np_s}F_{rn}(r)\cos[(np_s\theta_r+(np_s-p_r)\Omega t] - \sum_{\substack{n=qk+1\\k=0,1,2...}}\frac{J_n}{np_s}F_{rn}(r)\cos[(np_s\theta_r+(np_s+p_r)\Omega t]\right\} \quad (5)$$

where $F_{rn}(r)$ is a function of the radius r and space harmonic order n, and is given by

$$F_{rn}(r)=r\cdot\frac{1+\left(\frac{R_r}{r}\right)^{2np_s}}{1-\left(\frac{R_r}{R_s}\right)^{2np_s}}\left(\frac{r}{R_s}\right)^{np_s-1} \quad (6)$$

R_r is the radius of the rotor back-iron. The first and second terms in (5) are associated with the forward and backward rotating stator MMF harmonics, respectively. Assuming that the induced eddy current in the rotor magnets is resistance limited, the resultant eddy-current density J_e can be obtained from [6], [7]

$$J_e(r,\theta_r,t)=\frac{-1}{\rho}\frac{\partial A_z(r,\theta_r,t)}{\partial t}+C(t) \quad (7)$$

where ρ is the resistivity of the magnets. The second term in (7) is introduced to ensure that the net current which flows in each permanent-magnet arc segment of angle α is zero at any instant of time. It is therefore a function of time, and can be derived from

$$\int_{R_r}^{R_m}\int_{\alpha_i-\alpha/2}^{\alpha_i+\alpha/2}J_e(r,\theta_r,t)r\,dr\,d\theta_r=0 \quad (8)$$

where α_i is the angular displacement of the symmetric axis of the ith magnet segment referred in the rotor reference system. Substituting (5) into (7) and applying (8) yields the following expression for the eddy-current density in the ith magnet segment as shown in

$$\begin{aligned}J_{ei}(r,\theta_r,t) &= \frac{\Omega\mu_0 q}{2\rho}\cdot\left\{\sum_{n=qk-1;k=1,2,3...}\frac{J_n}{np_s}F_{rn}(r)(np_s-p_r)\sin[(np_s\theta_r+(np_s-p_r)\Omega t] - \sum_{n=qk+1;k=0,1,2...}\frac{J_n}{np_s}F_{rn}(r)(np_s+p_r)\sin[(np_s\theta_r+(np_s+p_r)\Omega t]\right\}\\ &+\frac{2\Omega\mu_0 q}{\alpha\rho\,(R_m^2-R_r^2)}\left\{-\sum_{n=qk-1;k=1,2,3...}I_n(np_s-p_r)\sin[(np_s\alpha_i+(np_s-p_r)\Omega t] + \sum_{n=qk+1;k=0,1,2...}I_n(np_s+p_r)\sin[(np_s\alpha_i+(np_s+p_r)\Omega t]\right\}. \quad (9)\end{aligned}$$

TABLE I
FREQUENCIES OF FORWARD AND BACKWARD ROTATING HARMONICS

Forward rotating, $n = 6k$-1, k = 2, 3, …	Backward rotating, $n = 6k$+1, k = 0, 1, 2,…	Frequency (normalised to $\Omega/2\pi$)
	1	6
	7	12
11		6
	13	18
17		12
	19	24
23		18
	25	30
29		24
	31	36

I_n is given by

$$I_n = \frac{2\sin(np_s\alpha/2)}{np_s}\int_{R_r}^{R_m}\frac{J_n}{np_s}F_{rn}(r)\,r\,dr = \frac{J_n}{n^2p_s^2}R_s^{-np_s+1}\left[\frac{R_m^{np_s+2}-R_r^{np_s+2}}{np_s+2} + R_r^{2np_s}\frac{R_m^{-np_s+2}-R_r^{-np_s+2}}{-np_s+2}\right]\sin\left(\frac{np_s\alpha}{2}\right). \quad (10)$$

The total eddy-current loss in the ith magnet segment can be obtained from

$$P_i = \frac{\Omega}{2\pi}\int_0^{2\pi/\Omega}\int_{R_r}^{R_m}\int_{\alpha_i-\alpha/2}^{\alpha_i+\alpha/2}\rho J_{ei}^2(r,\theta_r,t)\,r dr\,d\theta_r\,dt. \quad (11)$$

Using the orthogonal properties of trigonometric functions, the above integration in the published literatures on this subject is evaluated against each space harmonic and the result is obtained by summing their losses. However, the result is only correct if the frequency of the eddy current associated with each space harmonic is different. Unfortunately, this is not the case as will be evident from Table I which lists the frequencies of induced eddy current up to 31st space harmonics assuming, $q = 6, p_s = 1$ and $p_r = 5$.

As can be seen, a backward rotating harmonic of the order $n_b = [qk - (p_s + p_r - 1)]/p_s, (k = 1, 2, \ldots)$, and the forward rotating harmonic of the order $n_f = [qk + (p_s + p_r - 1)]/p_s$ induce two time-varying eddy-current harmonics of the same frequency $[qk - (p_s - 1)]\Omega/2\pi$ in the rotor magnets. For example, the backward rotating harmonic of order 1 and the forward rotating harmonic of order 11 have the same frequency of $3\,\Omega/\pi$. Consequently, the sum of the eddy-current loss components associated with each space harmonic may lead to an incorrect total eddy-current loss in a magnet segment. To circumvent this problem, the eddy-current density may be expressed in the form of sum of time harmonics

$$J_{ei}(r,\theta_r,t) = \sum_{k=1,2,\ldots}\{G_{nb}(r)\sin[(p_k-p_r)\theta_r + p_k\Omega t] + H_{nb}\sin[(p_k-p_r)\alpha_i + p_k\Omega t] + G_{nf}(r)\sin[(p_k+p_r)\theta_r + p_k\Omega t] + H_{nf}\sin[(p_k+p_r)\alpha_i + p_k\Omega t]\} \quad (12)$$

where $p_k = (qk - p_s + 1)$ and the definition for G_{nb}, G_{nf}, H_{nb}, and H_{nf} are given in Appendix A. It is evident that the four sine terms in (12) have the same frequency but different amplitude and phase angle, and the fundamental frequency of the induced eddy current is $(q - p_s + 1)\Omega/2\pi$. Substituting (12) into (11) and using the orthogonal property of trigonometric functions

$$\int_0^{2\pi}(\sin mx\cdot\sin nx)dx = \begin{cases}0 & m\neq n\\ \pi & m=n\end{cases} \quad (13)$$

the nonzero terms in the integration are given by

$$P_{ei} = P_0 + \rho\frac{\sin(p_r\alpha)}{p_r}\cos(2p_r\alpha_i)\sum_{k=1,2,3\ldots}G_{1k} \quad (14)$$

where P_0 is a loss component independent of the angular position of the ith segment, and can be evaluated using (8) given in [6]. Detailed derivation of (14) and definition of G_{1k} are given in Appendix B. The second term in (14) is proportional to $\cos(2p_r\alpha_i)$, and, hence, is dependent on the relative position of the segment within a pole pitch. It is also evident from the definition of G_{1k} in Appendix B that the summation term in (14) is a constant independent of the segment location.

It follows that if one magnet-pole is equally segmented into $N_{sg}(>1)$ pieces, the eddy-current loss in each piece may be different. This has two implications. i) The temperature distribution in the magnet segments will not be uniform, and the temperature will be higher in the segment with greater loss. Consequently, demagnetization risk will be increased [22]. ii) When the resistance limited model is employed to quantify 3-D eddy-current loss in PM brushless machines via magnetostatic analogy [23], the total loss cannot be determined by calculating loss in one magnet segment and multiplying the result by the number of segments. The number of segments to be calculated is dependent on the symmetry of the loss distribution and can be determined using (14).

The total eddy-current loss in the rotor magnets is given by

$$P_e = P_0(2p_rN_{sg}) + \rho\frac{\sin(p_r\alpha)}{p_r}\left\{\sum_{i=1}^{2p_rN_{sg}}\cos(2p_r\alpha_i)\right\}\sum_{k=1,2,3\ldots}G_{1k}. \quad (15)$$

Since

$$\alpha = \pi/(p_rN_{sg})\ \alpha_i = [\pi/N_{sg} + 2\pi(i-1)/N_{sg}]/(2p_r)$$

hence

$$\sum_{i=1}^{2p_rN_{sg}}\cos(2p_r\alpha_i) = 2p_r\sum_{i=1}^{N_{sg}}\cos\left(\frac{\pi}{N_{sg}} + \frac{2\pi}{N_{sg}}(i-1)\right) \equiv 0, \text{ if } N_{sg}\geq 2.$$

If $N_{sg} = 1$, or the magnet in one-pole is not segmented, $\alpha = \pi/p_r$ and $\sin(p_r\alpha) = 0$. Equation (15) can, therefore, be simplified to

$$P_e = P_0(2p_rN_{sg}). \quad (16)$$

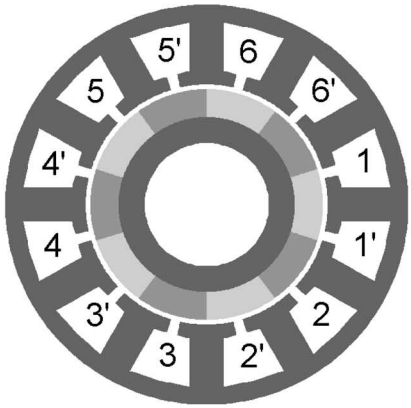

(a)

(b)

Fig. 1. Six-phase, 10-pole PM brushless machine. (a) Schematic. (b) Prototype.

TABLE II
DESIGN PARAMETERS AND SPECIFICATIONS

Stator outer diameter (mm)	130	Magnet outer radius (mm)	37.5
Machine active length (mm)	100	Magnet inner radius (mm)	28.43
Stator bore radius (mm)	39	Width of slot opening (mm)	1.5
Number of turn per coil	17	Rated current (peak A)	75.5
Rated speed (rpm)	5000	Magnet resistivity ($\mu\Omega$ m)	900

This result indicates that P_0 derived in [6] is, in fact, the average loss per pole of N_{sg} segmented pieces, albeit the loss in each segment may be different.

III. Validation by Finite-Element Analysis

To validate the analytical prediction, time-stepped 2-D transient FE analysis using Flux2D [24] was performed on a 6-phase, 10-pole PM brushless machine with modular windings, as shown in Fig. 1, whose design parameters are listed in Table II. Sm_2Co_{17} is used for the rotor magnets. Both the stator core and rotor back-iron were constructed using Transil 300 lamination sheets.

The magnetomotive force of the stator current in the machine contains a rich set of space harmonics, and the torque is produced by the interaction of the fifth harmonics with the field of 10-pole permanent magnets. The lower and higher order harmonics, which travel at different speeds with respect to the rotor, will induce significant eddy current and hence incur eddy-current loss in the magnets. Fig. 2 shows the geometry of the FE

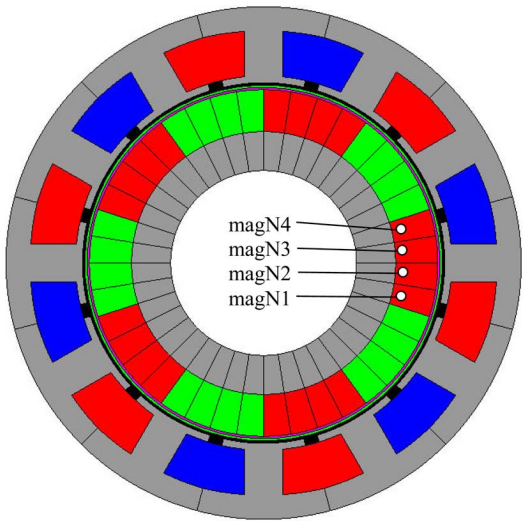

Fig. 2. Geometry of 2-D full model.

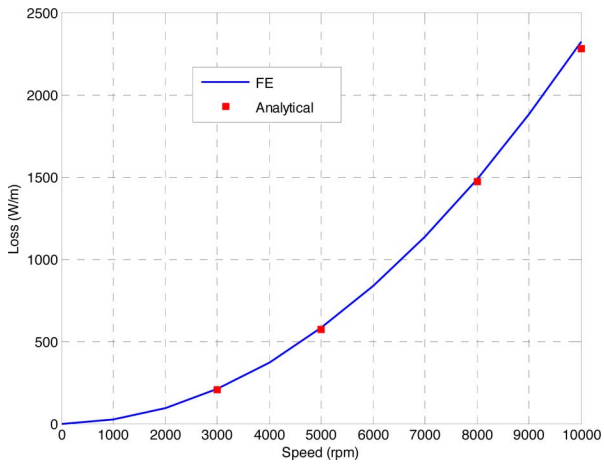

Fig. 3. Comparison of analytically and FE predicted variation of eddy-current loss per unit length with speed.

model in which the magnetic property of the stator and rotor cores is represented by the nonlinear BH curve of Transil 300 with their conductivity being set to zero. To reduce rotor eddy-current loss, each pole of magnets is segmented into four pieces. The 2-D FE model was solved when the six-phase windings were excited with the rated sinusoidal currents in phase with the back-electromotive forces (EMFs) and the rotor rotating at a constant speed. The time step was set to have 6 electric degrees for each step and the mesh size was adjusted such that the airgap flux density distributions were sufficiently smooth. Further, by assigning each magnet segment in Fig. 2 with a different region id, the Flux2D solver automatically assumes that each conducting region is insulated and the total current equal to zero constraint given in (8) is imposed. Fig. 3 compares analytically and FE predicted variations of eddy-current loss per unit length at full load with speed.

Figs. 4 and 5 show the resultant flux density and eddy-current distributions at $t = 0.125$ ms, respectively, when the rotor rotates at 5000 rpm. In all FE calculations, the remanence of the permanent magnets is set to zero, and the stator current waveforms are sinusoidal. That is, the eddy-current loss resulting

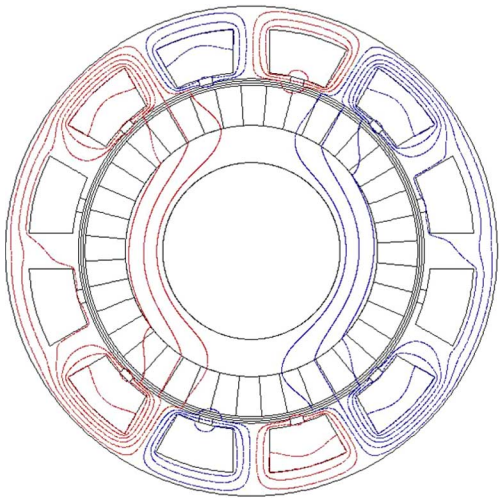

Fig. 4. Flux density distribution at $t = 0.125$ ms.

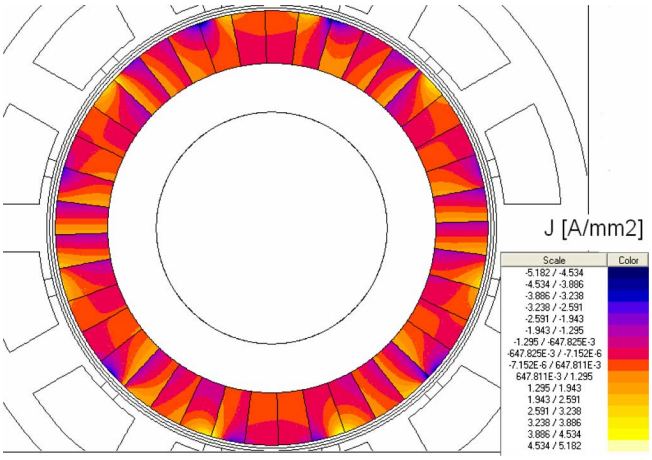

Fig. 5. Eddy-current distribution in rotor magnets at $t = 0.125$ ms.

from permeance variation due to slot opening and high order time harmonics in stator currents is not considered.

As will be seen from Fig. 4, the stator current excitation produces a 2-pole rotating magnetic field which can penetrate deeply into the rotor magnets, resulting in significant eddy-current loss if the magnets are not segmented. As the number of segments per pole increases, the eddy-current loss decreases. However for the machine under consideration, the rate of reduction in eddy-current loss diminishes as the number of segments is greater than 4. It is also evident that the analytically and FE predicted rotor eddy-current losses agree very well over a wide range of operating speed of the machine, which implies the resistance limited eddy-current model is sufficiently accurate up to the frequencies of concern in the machine.

Fig. 6 shows FE predicted variations of eddy-current losses with time over one fundamental eddy-current period in four segmented magnets within one-pole when the machine operates at 5000 rpm and full load. The positions of the magnets are shown in Fig. 1. As will be seen, the waveforms of the eddy-current losses in N1 and N2 are mirror images of those in N4 and N3, respectively. Thus, the average loss over one eddy-current period in N1 is equal to that in N4. The same relationship is true

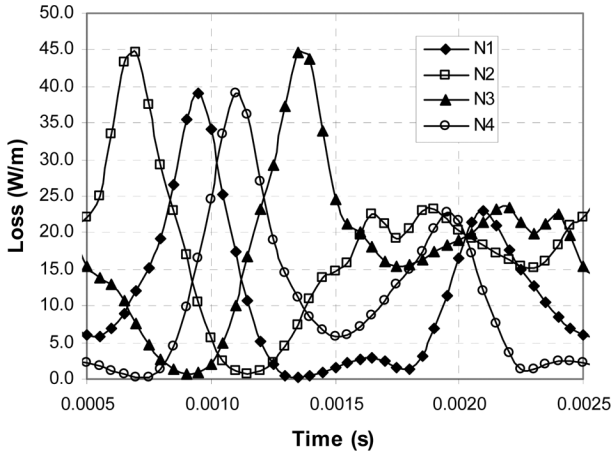

Fig. 6. Variation of eddy-current losses in four segments.

TABLE III
COMPARISON OF ANALYTICAL AND FE PREDICTED EDDY-CURRENT LOSS IN EACH SEGMENT

	FE (W/m)	Analytical (W/m)
N1	11.30	11.64
N2	17.84	18.39
N3	17.88	18.39
N4	11.30	11.64
Total loss per pole	58.32	60.06

for the average eddy-current loss in N2 and N3, i.e., the loss distribution is symmetrical to the central axis of the magnet pole. However, the loss in N2 and N3 is $\sim 45\%$ greater than that in N1 and N4. Table III compares the analytical and FE predicted eddy-current loss in the four magnet segments. A good agreement between the analytical and FE predictions is observed.

When the axial length of magnets is not significantly greater than its width and thickness, accurate evaluation of rotor eddy-current loss requires the use of 3-D time-stepped FE methods with rotor movement incorporated into the FE mesh. However, if the eddy current is resistance limited, the resultant eddy-current loss can be predicted using the magnetostatic analogy [23]. Since the eddy loss in equally segmented magnets is not the same, the total eddy-current loss cannot be evaluated by computing eddy-current loss in one segment. The number of magnet segments need to be modelled for 3-D magnetostatic calculation in order to predict the total eddy-current loss can be determined by (14) for a given number of segments per pole. For the example given in Fig. 1, magnetostatic field calculation needs to be performed in two segments.

IV. CONCLUSION

An analytical formula for predicting eddy-current loss in each segment of permanent-magnet brushless ac machines has been established. It has been shown that forward and backward rotating space harmonics of different orders may result in the same frequency seen by the rotor. Therefore, when more than two segments per pole are employed in PM machines, the loss in each segment may be significantly different. Such nonuniform distribution of eddy-current loss will inevitably give rise to uneven temperature distribution and increases the risk of partial irreversible demagnetization. It has been also shown that although previously reported analytical techniques

will adequately predict the average eddy-current losses in circumferentially segmented rotor permanent magnets, they are not suitable for predicting the eddy-current losses in individual segments when more than two segments per pole are employed. The theoretical derivation is validated by time-stepped transient FE analysis.

APPENDIX A

Definition of G_{nb}, G_{nf}, H_{nb}, and H_{nf} .

Let

$$c_1 = \frac{\Omega\mu_0 q}{2\rho}, c_2 = \frac{2\Omega\mu_0 q}{\alpha\left(R_m^2 - R_r^2\right)\rho}$$
$$p_k = qk - p_s + 1$$
$$G_{nb}(r) = -\frac{c_1 J_{nb} p_k}{p_k - p_r} F_{rnb}(r);$$
$$G_{nf}(r) = \frac{c_1 J_{nf} p_k}{p_k + p_r} F_{rnb}(r)$$
$$H_{nb} = c_2 I_{nb} p_k; H_{nf} = c_2 I_{nf} p_k$$

where $\{J_{nb,} J_{nf}\}$ and $\{F_{rnb}(r), F_{rnf}(r)\}$ are obtained by substituting for n in (2) and (6) with *nb* and *nf*, respectively. Similarly, I_{nb} and I_{nf} are obtained by substituting for n in equation (10) with *nb* and *nf*, respectively.

APPENDIX B

The average eddy-current loss in the ith segment can be evaluated by

$$\begin{aligned}
P_{ei} &= \frac{\Omega\rho}{2\pi}\int_0^{2\pi/\Omega}\int_{\alpha-\alpha_i/2}^{\alpha=\alpha_i/2}\int_{R_r}^{R_m} J_{ei}^2(r,\theta_r,t) r dr d\theta_r dt \\
&= \frac{\Omega\rho}{2\pi}\sum_{k=1,2,\ldots}\int_0^{2\pi/\Omega}\int_{\alpha-\alpha_i/2}^{\alpha=\alpha_i/2}\int_{R_r}^{R_m}\{(G_{nb}(r) \\
&\quad\times\sin[(p_k - p_r)\theta_r + p_k\Omega t] \\
&\quad + H_{nb}\sin[(p_k - p_r)\alpha_i + p_k\Omega t])^2 \\
&\quad + (G_{nf}(r)\sin[(p_k + p_r)\theta_r + p_k\Omega t] \\
&\quad + H_{nf}\sin[(p_k + p_r)\alpha_i + p_k\Omega t])^2\} r dr d\theta_r dt \\
&\quad + \frac{\Omega\rho}{\pi}\sum_{k=1,2,\ldots}\int_0^{2\pi/\Omega}\int_{\alpha-\alpha_i/2}^{\alpha=\alpha_i/2}\int_{R_r}^{R_m}\{(G_{nb}(r) \\
&\quad\times\sin[(p_k - p_r)\theta_r + p_k\Omega t] \\
&\quad + H_{nb}\sin[(p_k - p_r)\alpha_i + p_k\Omega t]) \\
&\quad\times(G_{nf}(r)\sin[(p_k + p_r)\theta_r + p_k\Omega t] \\
&\quad + H_{nf}\sin[(p_k + p_r)\alpha_i + p_k\Omega t])\} r dr d\theta_r dt. \qquad \text{(B.1)}
\end{aligned}$$

The first summation term yields the same result as that given by (8) in [5] while the second summation can be further simplified. Thus

$$P_{ei} = P_0 + \sum_{k=1,2,\ldots}(P_{1k} + P_{2k} + P_{3k} + P_{4k}) \qquad \text{(B.2)}$$

where

$$\begin{aligned}
P_{1k} &= \frac{\Omega\rho}{\pi}\sum_{k=1,2,\ldots}\int_0^{2\pi/\Omega}\int_{\alpha-\alpha_i/2}^{\alpha+\alpha_i/2}\int_{R_r}^{R_m}(G_{nb}(r) \\
&\quad\times\sin[(p_k - p_r)\theta_r + p_k\Omega t]) \\
&\quad\times(G_{nf}(r)\sin[(p_k + p_r)\theta_r + p_k\Omega t]) r dr d\theta_r dt \\
&= \frac{\rho\cos(2p_r\alpha_i)\sin(p_r\alpha)}{p_r} G_{1k} \\
G_{1k} &= \int_{R_r}^{R_m} G_{nb}(r) G_{nf}(r) r dr \qquad \text{(B.3)} \\
P_{2k} &= \frac{\Omega\rho}{\pi}\sum_{k=1,2,\ldots}\int_0^{2\pi/\Omega}\int_{\alpha-\alpha_i/2}^{\alpha+\alpha_i/2}\int_{R_r}^{R_m}(G_{nb}(r) \\
&\quad\times\sin[(p_k - p_r)\theta_r + p_k\Omega t]) \\
&\quad\times(H_{nf}\sin[(p_k + p_r)\theta_r + p_k\Omega t]) r dr d\theta_r dt \\
&= \frac{2\rho\cos(2p_r\alpha_i)\sin[(p_k - p_r)\alpha/2]}{p_k - p_r}\int_{R_r}^{R_m} G_{nb}(r) H_{nf} r dr \\
&= \rho c_1 c_2 p_k^2 I_{nf} I_{nb}\cos(2p_r\alpha_i) \qquad \text{(B.4)} \\
P_{3k} &= \frac{\Omega\rho}{\pi}\sum_{k=1,2,\ldots}\int_0^{2\pi/\Omega}\int_{\alpha-\alpha_i/2}^{\alpha+\alpha_i/2}\int_{R_r}^{R_m}(G_{nf}(r) \\
&\quad\times\sin[(p_k + p_r)\theta_r + p_k\Omega t]) \\
&\quad\times(H_{nb}\sin[(p_k - p_r)\theta_r + p_k\Omega t]) r dr d\theta_r dt \\
&= \frac{2\rho\cos(2p_r\alpha_i)\sin[(p_k + p_r)\alpha/2]}{p_k + p_r}\int_{R_r}^{R_m} G_{nf}(r) H_{nb} r dr \\
&= \rho c_1 c_2 p_k^2 I_{nf} I_{nb}\cos(2p_r\alpha_i) \qquad \text{(B.5)} \\
P_{4k} &= \frac{\Omega\rho}{\pi}\sum_{k=1,2,\ldots}\int_0^{2\pi/\Omega}\int_{\alpha-\alpha_i/2}^{\alpha+\alpha_i/2}\int_{R_r}^{R_m}(H_{nf} \\
&\quad\times\sin[(p_k + p_r)\alpha_i + p_k\Omega t]) \\
&\quad\times(H_{nb}\sin[(p_k - p_r)\alpha_i + p_k\Omega t]) r dr d\theta_r dt \\
&= \rho H_{nb} H_{nf}\cos(2p_r\alpha_i)\frac{\alpha\left(R_m^2 - R_r^2\right)}{2} \\
&= -\rho\frac{\alpha\left(R_m^2 - R_r^2\right)}{2}\cos(2p_r\alpha_i) c_2^2 p_k^2 I_{nf} I_{nb}. \qquad \text{(B.6)}
\end{aligned}$$

However, the sum of P_{2k}, P_{3k}, and P_{4k} are given by

$$\begin{aligned}
P_{2k} + P_{3k} + P_{4k} &= \rho\cos(2p_r\alpha) I_{nf} I_{nb} p_k^2 \\
&\quad\times\left[2c_2 c_1 - \frac{\alpha(R_m^2 - R_r^2)}{2} c_2^2\right] = 0. \qquad \text{(B.7)}
\end{aligned}$$

Substituting (B.3) and (B.7) into (B.2) yields (14).

REFERENCES

[1] A. Fratta, A. Vagati, and F. Villata, "On the evolution of AC machines for spindle drive applications," *IEEE Trans. Ind. Appl.*, vol. 28, no. 5, pp. 1081–1086, Sep.–Oct. 1992.

[2] Z. Q. Zhu and D. Howe, "Electrical machines and drives for electric, hybrid and fuel cell vehicles," *Proc. IEEE*, vol. 95, no. 4, pp. 746–765, Apr. 2007.

[3] J. Wang, K. Atallah, Z. Q. Zhu, and D. Howe, "Modular 3-phase permanent magnet brushless machines for in-wheel applications," *IEEE Trans. Veh. Technol.*, vol. 57, no. 5, pp. 2714–2720, 2008.

[4] Y. Chen, P. Pillay, and A. Khan, "PM wind generator topologies," *IEEE Trans. Ind. Appl.*, vol. 41, no. 6, pp. 1619–1626, 2005.

[5] X. Sun, C. Ming, W. Hua, and L. Xu, "Optimal design of double-layer permanent magnet dual mechanical port machine for wind power application," *IEEE Trans. Magn.*, vol. 45, no. 10, pp. 4613–4616, Oct. 2009.

[6] K. Atallah, D. Howe, P. H. Mellor, and D. A. Stone, "Rotor loss in permanent-magnet brushless AC machines," *IEEE Trans. Ind. Appl.*, vol. 36, no. 6, pp. 1612–1618, Nov./Dec. 2000.

[7] H. Polinder and M. J. Hoeijmarkers, "Eddy current losses in the segmented surface-mounted magnets of a PM machine," *Proc. Inst. Elect. Eng.*, vol. 146, no. 3, pp. 261–266, May 1999.

[8] H. Toda, Z. P. Xia, J. Wang, K. Atallah, and D. Howe, "Rotor eddy current loss in permanent magnet brushless machines," *IEEE Trans. Magn.*, vol. 40, no. 4, pp. 2104–2106, Jul. 2004.
[9] Y. Amara, J. Wang, and D. Howe, "Analytical prediction of eddy current loss in modular tubular permanent magnet machines," *IEEE Trans. Energy Convers.*, vol. 20, no. 4, pp. 761–770, 2005.
[10] D. Ishak, Z. Q. Zhu, and D. Howe, "Eddy-current loss in the rotor magnets of permanent-magnet brushless machines having a fractional number of slots per pole," *IEEE Trans. Magn.*, vol. 41, no. 9, pp. 2462–2469, Sep. 2005.
[11] F. Deng, "Commutation-caused eddy-current losses in permanent magnet brushless dc motors," *IEEE Trans. Magn.*, vol. 33, no. 5, pp. 4310–4318, Sep. 1997.
[12] F. Deng, "Analytical modeling of eddy current losses caused by pulse width-modulation switching in permanent-magnet brushless dc motors," *IEEE Trans. Magn.*, vol. 34, no. 5, pp. 3728–3736, Sep. 1998.
[13] Z. Q. Zhu, K. Ng, N. Schofield, and D. Howe, "Improved analytical modelling of rotor eddy current loss in brushless machines equipped with surface mounted permanent magnets," *Proc. Inst. Elect. Eng.*, vol. 151, no. 6, pp. 641–650, Nov. 2004.
[14] M. R. Shah and S. B. Lee, "Rapid analytical optimization of eddy-current shield thickness for associated loss minimization in electrical machines," *IEEE Trans. Ind. Appl.*, vol. 42, no. 3, pp. 642–649, May–Jun. 2006.
[15] M. R. Shah and S. B. Lee, "Optimization of shield thickness of finite length rotors for eddy current loss minimization," in *Proc. IEEE Industry Applications Soc. 41st Annual Meeting*, Oct. 2006, paper IAS60p2.
[16] M. R. Shah and A. M. EL-Refaie, "Eddy current loss minimization in conducting sleeves of high speed machine rotors by optimal axial segmentation and copper cladding," in *Proc. IEEE Industry Applications Soc. 42nd Annual Meeting*, Oct. 2007.
[17] K. Yoshida, K. Kesamaru, and Y. Hita, "Eddy currents analysis of surface-mounted PMSM by finite element method," in *Proc. Int. Conf. on Electrical Machines*, Istanbul, Turkey, 1998, pp. 1821–1825.
[18] N. Shuangxia Chau, K. T. Chau, and J. Z. Jiang, "Analysis of eddy-current loss in a double-stator cup-rotor PM machine," *IEEE Trans. Magn.*, vol. 44, no. 11, pp. 4401–4404, Nov. 2008.
[19] S. Ruoho, T. Santa-Nokki, J. Kolehmainen, and A. Arkkio, "Modeling magnet length in 2-D finite-element analysis of electric machines," *IEEE Trans. Magn.*, vol. 45, no. 8, pp. 3114–3120, Aug. 2009.
[20] G. J. Atkinson, B. C. Mecrow, A. G. Jack, D. J. Atkinson, P. Sangha, and M. Benarous, "The analysis of losses in high-power fault-tolerant machines for aerospace applications," *IEEE Trans. Ind. Appl.*, vol. 42, no. 5, pp. 1162–1170, 2006.
[21] P. Sergeant, P. , and A. Van den Bossche, "Segmentation of magnets to reduce losses in permanent-magnet synchronous machines," *IEEE Trans. Magn.*, vol. 44, no. 11, pp. 4409–4412, Nov. 2008.
[22] J. Wang, W. Wang, K. Atallah, and D. Howe, "Demagnetization assessment for 3-phase tubular brushless permanent magnet machines," *IEEE Trans. Magn.*, vol. 44, no. 9, pp. 2195–2203, 2008.
[23] J. D. Ede, K. Atallah, G. Jewell, J. Wang, and D. Howe, "Effect of axial segmentation of permanent magnets on rotor loss in modular permanent magnet brushless machines," *IEEE Trans. Ind. Appl.*, vol. 43, no. 5, pp. 1207–1213, Sep./Oct. 2007.
[24] Flux2D/Flux3D Version 10.1 User Manual 2008, Cedrat.

Jiabin Wang (SM'03) received the B.Eng. and M.Eng. degrees from Jiangsu University of Science and Technology, Zhengjiang, China, in 1982 and 1986, respectively, and the Ph.D. degree from the University of East London, London, U.K., in 1996, all in electrical and electronic engineering.

Currently, he is a Reader in electrical engineering at the University of Sheffield, Sheffield, U.K. From 1986 to 1991, he was with the Department of Electrical Engineering, Jiangsu University of Science and Technology, where he was appointed a Lecturer in 1987 and an Associate Professor in 1990. He was a Postdoctoral Research Associate at the University of Sheffield, Sheffield, U.K., from 1996 to 1997, and a Senior Lecturer at the University of East London from 1998 to 2001. His research interests extend from motion control to electromagnetic devices and their associated drives in applications ranging from automotive, household appliances to aerospace sectors.

Kais Atallah received the Ingenieur d'Etat degree in electrical power engineering from Ecole Nationale Polytechnique, Algeria, and the Ph.D. degree from the University of Sheffield, Sheffield, U.K.

From 1993 to 2000, he was a Research Associate in the Department of Electronic and Electrical Engineering, University of Sheffield, where he is currently a Senior Lecturer. His research interests embrace fault-tolerant permanent magnet drives for aerospace, magnetic gearing, and "pseudo" direct drive electrical machines. He is a co-founder of the University spin-off company, Magnomatics, Ltd.

Robert Chin received the B.Sc degree in electromechanical engineering from the University of Cape Town, South Africa, in 1997 and the M.Sc and Ph.D. degrees in electrical power engineering from the Royal Institute of Technology, Stockholm, Sweden, in 2001 and 2006, respectively.

He is currently a Research Engineer with ABB Corporate Research, Västerås, Sweden. His main research interests are in the fields of electric machines and renewable energy technologies.

Dr. Chin is the IEEE IAS Sweden Chapter Chair.

Waqas M. Arshad received the B.Sc. Eng. degree from the University of Taxila, Pakistan, and the M.S. and Ph.D. degrees from the Royal Institute of Technology, Stockholm, Sweden.

He has been a Group Manager for power electronics and machines at ABB US Corporate Research Center, Raleigh, NC, since October 2008. Prior to this assignment, he was with ABB Sweden Corporate Research Centre, Västerås, Sweden.

Heinz Lendenmann received the B.Sc. Eng. degree from Neu Technikum Buchs, Switzerland. He received the M.Sc. and Ph.D. degrees in electrical engineering from the University of Arizona, Tucson, and the Swiss Institute of Technology, ETH Zürich, in 1990 and 1994, respectively.

From 1998 to 2002, he was active in silicon carbide research and co-/authored several scientific publications on the topic. He leads a research group in Power Electronics and Electrical Machines and is now responsible for Wind Technologies at ABB Corporate Research, Västerås, Sweden.